Temperature dependence of the optically induced production and annealing of silicon dangling bonds in hydrogenated amorphous silicon

N. A. Schultz and P. C. Taylor
Department of Physics, University of Utah, Salt Lake City, Utah, 84112
(Received 12 March 2002; published 7 June 2002)

In hydrogenated amorphous silicon the kinetics of the optically induced production and thermal annealing of silicon dangling bonds have been measured at temperatures between 25 and 480 K using electron spin resonance (ESR). Below about 150 K the measurement of optically induced silicon dangling bonds is masked by long-lived, band-tail carriers that accumulate with time t as $t^{1/3}$. It is known that these long-lived carriers can be quenched by infrared light. However, optically, it is not possible to completely remove them. The production rate for optically induced silicon dangling bonds decreases with decreasing temperature. Below about 100 K degradation is at most half as efficient as at room temperature and is nearly temperature independent below approximately 100 K. Additionally, defects created by 10 h of irradiation below 100 K almost entirely anneal at $T \cong 300$ K. It is common procedure to anneal *a*-Si:H samples for 30 min at 175 °C to restore the as-deposited defect density. However, by repeatedly performing degradation and annealing cycles we find that a small fraction of defects is not restored by annealing at 175 °C and that these defects slowly accumulate with degradation. For defects created at all temperatures we find the same ESR fingerprint, indicating that only one dominant type of defect is created, presumably the silicon dangling bond, and we conclude that different, temperature-dependent stabilization processes must exist. These results lead to new constraints for models that attempt to explain the Staebler-Wronski effect.

DOI: 10.1103/PhysRevB.65.235207 PACS number(s): 78.66.Jg, 72.80.Ng, 61.72.Cc, 76.30.−v

INTRODUCTION

Most amorphous solids exhibit metastabilities in their electronic or optical properties. These metastabilities exist because the amorphous phase is not an equilibrium configuration. In the amorphous semiconductors the prototypical example is hydrogenated amorphous silicon (*a*-Si:H), and the prototypical metastability is that which underlies the Staebler-Wronski effect (SWE).[1] The Staebler-Wronski effect is a metastable, optically induced degradation of the photoconductivity and dark conductivity. The SWE is commonly attributed to the optically induced production of metastable silicon dangling bonds,[2] i.e., undercoordinated Si atoms with energy levels within the gap. Generally, other effects, such as the degradation of *a*-Si:H solar cell efficiencies, are also interpreted as manifestations of the SWE. From the electron spin resonance (ESR) line shape whose g value from the zero crossing of the derivative spectrum is $g = 2.055$,[3] from an observed proportionality between the low-energy optical absorption and the ESR,[4] and from the hyperfine interaction with ^{29}Si in enriched samples,[5] many researchers have concluded that the optically induced spins originate from silicon dangling bonds. Therefore, the ESR resonance at $g \sim 2$ is a measure for the dangling bond density, and hence its increase is commonly taken as a quantitative measure for the degradation of *a*-Si:H. It is well known that optically induced degradation is a reversible process. Annealing the sample at temperatures of about 150–200 °C for about 30 min is the common procedure to restore the original defect density of the as-deposited sample. This cycle of optically induced degradation and annealing can be repeated many times without long-term, irreversible changes.[6]

The creation of the metastability involves the diffusion of hydrogen.[7] In particular, it is often assumed that hydrogen motion is involved in the dangling bond stabilization process. Therefore, an understanding of the kinetics for the production of silicon dangling bonds is very important to any microscopic description of the SWE. Because the optically induced generation of silicon dangling bonds is a very inefficient process, it is probable that larger densities of additional, different defects are formed by the motion of hydrogen.[8,9] There may even be some irreversible effects.[4,10] Photoconductivity experiments[6,11] at low temperatures have suggested that the SWE is only weakly dependent on temperature below 300 K; i.e., the low-temperature production of dangling bonds is about 70% as efficient as at room temperature. Although hydrogen motion is likely to be greatly suppressed at low temperatures, an optically enhanced diffusion mechanism that is essentially temperature independent has been proposed.[12] This mechanism of optically enhanced diffusion of hydrogen may result from energetically favorable nonradiative recombination processes.[13] In this paper we show that below approximately 300 K the production of silicon dangling bonds shows a marginally stronger dependence on the temperature than previously observed, i.e., that the production below approximately 100 K is at most half as efficient as at 300 K. In addition, the dangling bonds produced by up to 10 h of irradiation below 100 K are unstable and anneal essentially completely at 300 K. The existing kinetic models that attempt to explain the SWE are not complete enough to explain this complex behavior. We suggest that the silicon dangling bond production can be separated into two steps. First, silicon dangling bonds are produced essentially independently of temperature, presumably mediated by optically excited carrier recombination. Second, there follows a stabilizing process that involves hydrogen

migration. The stabilizing process must be temperature dependent.

It is well known[14] that below about 150 K a subset of the optically excited carriers can live for very long times, some of which easily exceed several hours. Some of these long-lived carriers can be induced to recombine (the densities can be quenched) by irradiation of the sample with low-energy, infrared light. The assumption is that the lower-energy infrared light reexcites the carriers trapped in the band tails and therefore promotes diffusion and recombination of electrons and holes. This mechanism is inferred from changes induced by infrared light in photoluminescence (PL),[15] optically induced ESR (LESR),[15] and photoconductivity (PC).[6,16,17] However, PL and PC provide no microscopic information on the defects, and the standard detection of LESR is not sensitive enough to study the bleaching kinetics in any detail. Therefore, the connections of these experiments with specific models have necessarily involved considerable conjecture. The present LESR results provide direct information on both the microscopic origins of the optically induced defects and the kinetics for their production and decay. In particular, although previous PC experiments[17–19] suggested that infrared light completely removed the band-tail carriers at low temperatures, the present results show that a significant fraction of the long-lived carriers is not affected by the quenching light on a laboratory time scale ($t < 10^4$ s).

EXPERIMENT

Detailed kinetic experiments using ESR and LESR at low temperatures are difficult due to saturation of the LESR signal as a result of long spin-lattice relaxation times. Recently, Yan *et al.*[20,21] have employed a second-harmonic detection technique that effectively eliminates this difficulty and allows for detailed kinetic experiments to be performed, even for small ESR spin densities. In this technique the ESR signal is detected at twice the magnetic field modulation frequency, which was set to 50 kHz. The improvement in effective signal-to-noise ratio can be several orders of magnitude at low temperatures. Whereas the standard detection of ESR results in a signal proportional to the derivative of the absorption, the second-harmonic detection results in a line shape that roughly approximates the resonant absorption component. Details are available elsewhere.[20]

All experiments were performed on a standard ESR spectrometer (Bruker) at the *X* band. The sample was mounted inside an ESR cavity equipped with openings to irradiate the sample inside the cavity. Except where otherwise stated, ESR experiments were performed at about 40 K. For the experiments to measure the excitation and bleaching of electrons and holes trapped in localized band-tail states, the sample consisted of *a*-Si:H flakes confined in a quartz sample tube. The sample volume was approximately 1.5×10^{-3} cm^3, and the dark ESR spin density due to residual silicon dangling bonds was approximately 2×10^{16} cm^{-3}. A HeNe laser (approximately 3 mW/cm^2 at 6328 Å at the sample) was employed as the excitation source. A glowbar with long-wavelength pass filters was used for all infrared bleaching of the optically excited carriers (approximately 0.5 mW/cm^2 at the sample with a 2500-nm-long pass filter or approximately 10^{18} photons cm^{-2} s^{-1}).

The sample of *a*-Si:H, which was employed to study the optically induced production of silicon dangling bonds, consisted of four stacked films of *a*-Si:H on quartz substrates. The *a*-Si-H films, which had a total thickness of approximately 10 μm, had a dark ESR spin density of less than 2×10^{16} cm^{-3}. This estimate includes the spins on the eight surfaces, and therefore the bulk spin density is considerably less. For these experiments, light from a Xe arc lamp through an orange filter (approximately 0.5 W/cm^2 at the sample) was employed as the excitation source. In every degradation measurement the sample was irradiated for 10 h. Annealing of the sample at temperatures *T* below 300 K took place inside the cavity by reduction of the cooling He gas flow. After every 10-h degradation measurement the sample was removed from the cavity and annealed at 175 °C for 30 min in a nitrogen atmosphere. At room temperature, 10 h of illumination increased the spin density by about 150% relative to the spin density of the as-deposited sample.

RESULTS

The LESR signals due to optically excited electrons and holes trapped in localized band-tail states are superimposed on the ESR signal ascribed to silicon dangling bonds. The two ESR responses attributed to band-tail electrons and holes occur at *g* values of approximately 2.004 and 2.01, respectively, while the signal attributed to silicon dangling bonds occurs at approximately 2.0055.[3] Because the linewidths for all three resonances are several gauss, the ESR responses due to band-tail electrons and silicon dangling bonds are difficult to resolve experimentally. We therefore first examine the kinetics and efficiencies for infrared and thermal bleaching of the LESR signals attributed to band-tail electrons and holes. To examine the efficiency for IR quenching of the optically excited carriers we cooled the sample in the dark to avoid any early optical excitation and set the magnetic field to the resonant field of the optically excited electrons ($g\sim2.004$). At this magnetic field the measured ESR signal also contains contributions of the dark-spin ESR signal, which is ascribed to silicon dangling bonds. Since we are interested in the kinetics of the long-lived, optically excited carriers only, we subtracted this background ESR signal. For this reason, the ESR signal for the optically excited carriers at time $t=0$ is zero in Fig. 1. We recorded the ESR signal, i.e., the dark-spin density, for approximately 1 min and then started the optical excitation.

At the optical excitation intensity used, the optically induced LESR signal rapidly increased and was followed by a very much slower component that continued to rise for many hours. At stronger light intensities the rise of the LESR signal to saturation approximated a step function. After about 20 min of optical excitation, when the optically excited carrier density reached approximately a steady-state value on a time scale of minutes, we turned off the optical excitation and monitored the decay of the optically excited carriers in the dark. An initial rapid decay was followed by a very much

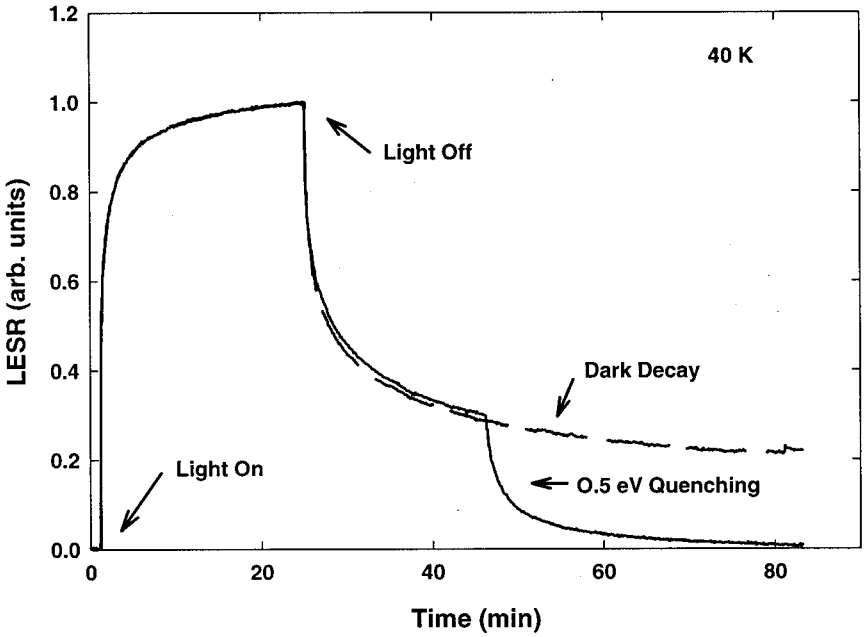

FIG. 1. Growth and decay of the optically induced electron spin resonance signal after turning the optical excitation (photon energy approximately 2 eV) on and off, respectively, and optically induced quenching (photon energy approximately 0.5 eV) of the long-lived optically induced carriers. See text for details.

slower component that was still detectable after many hours (upper curve in Fig. 1).

To examine the efficiency of optically induced quenching we repeated this cycle, but after the dark decay had almost reached a steady-state value on a time scale of minutes, i.e., at about 45 min, we illuminated the sample with approximately 0.5 eV light (lower curve in Fig. 1). A rapid decay immediately occurred, which again was followed by a very slow component that remained detectable for many hours. This initial, rapid decay has also been observed in previous transient, ir-optically induced photoluminescence[15] and photoconductivity[22,23] experiments. The ir-induced decay to a new, lower steady-state value was observable using 0.5 ± 0.2 eV light. However, at no energy were we able to totally quench all carriers. Lower quenching energies were less efficient and resulted in a slightly higher ir-quenched steady-state carrier density. We could not test ir-quenching energies less than 0.4 eV because we were limited by the transmission properties of the quartz sample tube. Quenching energies a few tenths of an eV higher than 0.5 eV resulted in decay curves very similar to the one shown in Fig. 1.

There was an interesting transition region near 1 eV. For excitation energies well above 1 eV the light always increased the densities of carriers trapped in the band-tail states. However, when illuminating the sample with about 1.1 eV during decay in the dark, the behavior of the ESR signal depended on the history of the sample. Illuminating the sample with 1.1 eV soon after the initial high-energy optical excitation was turned off produced a quenching of the signal. At later times, when the ESR signal had further decayed in the dark, illumination at 1.1 eV produced an increase in the signal to a higher steady-state value. This increase is probably due to a two-step excitation process that is prominent in PL excitation experiments.[24,25] In summary, although optically induced quenching at 0.5 eV is an efficient means to remove long-lived carriers, a small but significant fraction clearly survives the ir quenching and appears to follow the same dark decay as the unquenched carriers.

Since ir light does not fully quench the long-lived carriers, we examined the accumulation of these very-long-lived, band-tail carriers after many inducing and quenching cycles. Initially we cooled down the sample in the dark and performed an ESR measurement (lowest curve in Fig. 2). We then went through the following inducing and quenching cycle many times: (1) We irradiated the sample for a certain amount of time ($30\ \mathrm{s} < t < 3600\ \mathrm{s}$) that approximately doubled in every cycle. (2) We irradiated the sample for 3 min with 0.5 eV light to quench the short-lived, band-tail carriers and to emphasize the accumulation of long-lived carriers. This quenching procedure is very similar to that used in previous photoconductivity experiments.[17–19] After ir quenching we kept the sample in the dark for approximately 10 min to establish an approximate equilibrium LESR density (on a time scale of minutes). By following this procedure we minimized the influence of any thermal relaxation during the subsequent measurement of the remaining LESR signals. In any case, small thermal decays during the ESR measurement tend to affect all measurements in a similar fashion.

Figure 2 shows these ESR measurements after successive irradiation and quenching cycles. The small feature just below 3400 G is an artifact and is due to E' centers[26] on the quartz substrates or in the quartz insert Dewar. It is clear from Fig. 2 that the more stable band-tail carriers, i.e., those that cannot be bleached with ir light, accumulate after cycling. The long-lived carriers, as can be seen in the inset to Fig. 2, grow approximately as a power law in time t as $t^{1/3}$ until saturation. This dependence on time is often observed for the creation of silicon dangling bonds at room temperature,[27] but in the present case the signal is exclusively due to electrons and holes that are deeply trapped in localized, band-tail states. This conclusion follows unambiguously from the ESR line shape that clearly shows a

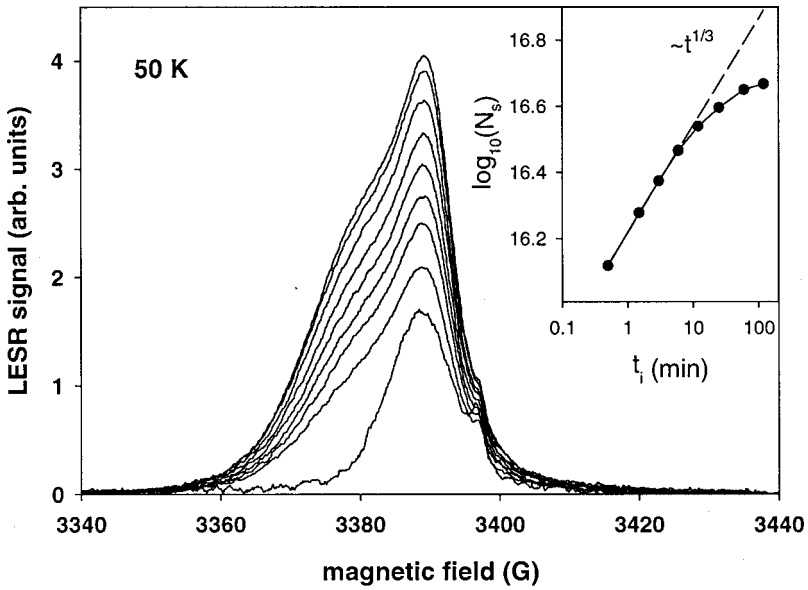

FIG. 2. Accumulation of long-lived carriers. Between two consecutive ESR measurements the sample was illuminated with 2 eV light, exposed to 0.5 eV light for 3 min, and kept for 10 min in the dark. The smallest spectrum shows the dark ESR due to silicon dangling bonds. Inset: increase of long-lived carriers relative to the dark ESR signal. The abscissa of the inset shows the total illumination time.

shoulder on the low-field side, which is ascribed to holes trapped in valence band-tail states.

Next, we examine the kinetics for the production of silicon dangling bonds at temperatures between 25 and 300 K. At low temperatures it is very difficult to distinguish between the optically excited, long-lived carriers and the silicon dangling bonds. Therefore, to minimize the influence of long-lived, band-tail carriers we performed an ir-quenching cycle after every low-temperature degradation cycle ($T<150$ K). The ir-quenching provided an upper limit on the actual number of optically induced dangling bonds. We performed the following measurements: (1) We mounted a freshly annealed sample inside the ESR cavity and cooled to 40 K. (2) We measured the dark-spin density to prove that the spin density of the sample was approximately the same as in the as-deposited state. (3) We degraded the sample for 10 h at degradation temperatures T_{deg} of 25, 40, 100, and 170 K. (4) After each degradation cycle we measured the spin density (i) immediately following ir-quenching for approximately 5 min and after annealing at (ii) 120 K, (iii) 220 K, and (iv) 300 K inside the cavity. For the sample, which was degraded at 170 K, annealing at 120 K was not applicable, since T_{deg} was higher than 120 K. After irradiation at 25 K, the ESR measurements were performed at 25 K. All other ESR measurements were performed at 40 K to eliminate the influence of temperature on the ESR intensity. (5) After every low-temperature degradation experiment, including ir quenching and low-temperature annealing, we removed the sample from the cavity and annealed it in a nitrogen atmosphere at 175 °C for 30 min. (6) After all low-temperature degradation and annealing cycles were completed, we mounted the sample inside the ESR cavity and degraded the sample at 300 K for 10 h. For this 300 K degradation cycle, we measured the initial and final spin concentrations at 40 K.

In Fig. 3 the optically induced spin concentrations at low temperature are shown relative to the optically induced spin concentrations at room temperature. The abscissa is proportional to the inverse of the degradation temperature T_{deg}. Here ESR measurements performed after the same quenching process, i.e., after ir quenching (triangles) or annealing at 220 K (bullets) or 300 K (squares), are connected with lines. The error bars represent statistical errors of the individual ESR measurements. However, other influences, such as small differences in sample positioning inside the cavity for the low-T and subsequent room-temperature degradations, are not taken into account. Within the error bars the number of optically induced spins that where produced at $T<100$ K and measured after ir quenching are very similar to those measured after annealing at 120 K. Therefore, only the optically induced spin densities after ir quenching are shown in Fig. 3.

Two conclusions are obvious from the data shown in Fig. 3. First, from the spin densities measured after ir quenching (triangles), we conclude that degradation at 100, 50 and 25 K is at most half as efficient as at room temperature. Second, annealing the sample at 220 K (bullets) and 300 K (squares) significantly reduces the spin density, indicating that significant annealing starts at temperatures well below 300 K. Note the overlap with zero for the error bars of the ESR measurements that where performed after annealing at 300 K. This behavior shows that the spins created at low temperatures ($T<100$ K) are almost entirely, if not entirely, annealed at 300 K.

The inset to Fig. 3 shows an experiment[10] with a similar experimental procedure as in the present work. For these data (squares) a different sample was used and laser excitation was employed. After every degradation measurement the sample was annealed at approximately 250 K and all ESR measurements were performed at the degradation temperature. These data are compared to the data of the present work (Fig. 3), where the annealing temperature was about 220 K (bullets) and the LESR measurements were performed at 40 K. Only small differences that we ascribe to systematic errors are observable. This result indicates that the choices of sample and experimental parameters do not significantly influence the results.

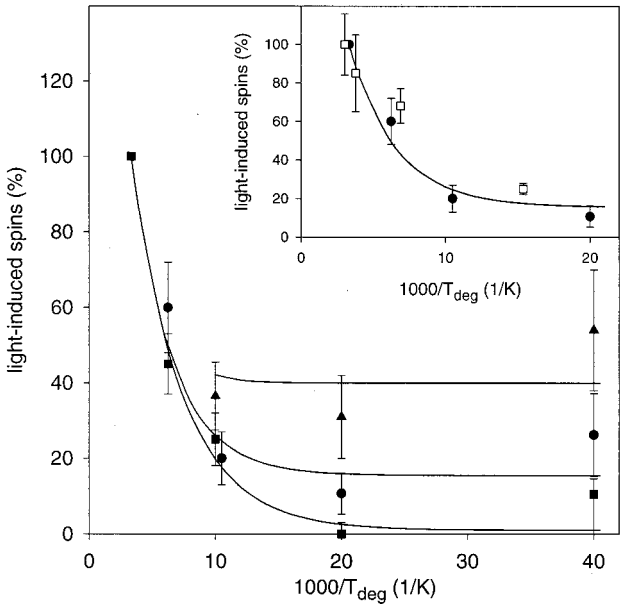

FIG. 3. Optically induced increase in spin density after 10 h of illumination at temperatures lower than room temperature. The abscissa shows the inverse of the degradation temperature. After every illumination period the ESR spin density was measured after ir quenching (triangles) and after annealing at 220 K (circles) and 300 K (squares). All ESR measurements were made at 40 K, except for the sample degraded at 25 K, which was measured at 25 K. The inset shows the temperature-dependent increase of optically induced spins measured at the degradation temperatures after annealing at about 250 K (squares) compared to degradation data of the main figure, where the measurement temperature was 40 K and the annealing temperature was 220 K (circles). All optically induced increases in spin densities are shown relative to the increase at room temperature, and the lines are guides to the eye.

The annealing kinetics are shown in Fig. 4, which contains the data of Fig. 3 plotted as a function of the annealing temperature. The annealing behavior of the sample degraded at room temperature is also shown for comparison. For this latter measurement the degraded sample was annealed for 1 h at subsequently higher temperatures and measured at room temperature. From these room-temperature measurements one can see the commonly observed result[27] that significant annealing sets in at temperatures above about 390 K. Annealing at 420 K almost fully restores the initial spin density of the as-grown sample. As already seen, the optically induced spin densities after 10 h of degradation at 25 K (upward pointing triangles), 50 K (squares), and 100 K (circles), all followed by ir quenching, are the same within experimental error. The magnitude of the degradation is about 50% of the optically induced degradation at 300 K. Since the spin densities of these samples show a very similar behavior, only one line is shown as a guide to the eye for these samples. For the degradations at 100 K or below, annealing the sample for a few minutes at higher temperatures (120, 220, and 300 K) shows that only a small fraction of the degradation survives annealing at 300 K. The overlap of the error bars at 300 K with zero indicates that possibly all defects that were created at temperatures below about 100 K anneal at 300 K. Among

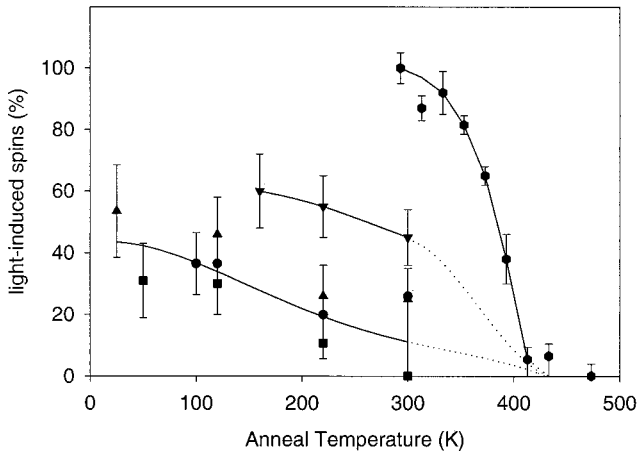

FIG. 4. Temperature-dependent annealing of defects created at temperatures between 25 and 300 K. Optically induced defects created at low temperatures (up triangles: 25 K, squares: 50 K, circles: 100 K) anneal at much lower temperatures than defects created at higher temperatures (down triangles: 170 K, hexagons: 300 K). The lines are guides to the eye.

the spins produced at 170 K (downward pointing triangles), a significant fraction survives annealing at 300 K. The dotted lines illustrate the expected extrapolations such that all optically induced spin densities anneal at about 420 K.

The described measurements that lead to Figs. 3 and 4 are the result of many ESR spin density measurements of a frequently degraded and annealed *a*-Si:H sample. Figure 5 gives an overview of the ESR spin densities after every annealing process for 30 min at 175 °C (downward pointing triangles) and after every room-temperature degradation process (upward pointing triangles), i.e., the initial and final spin densities before and after each degradation and annealing

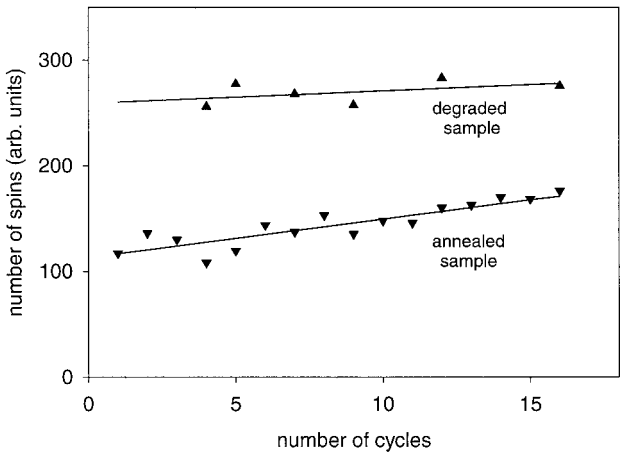

FIG. 5. ESR spin densities of one sample as measured several times after annealing (30 min, 175 °C) and 10-h room-temperature degradation. The scatter in the data is ascribed to slightly varying positions of the sample inside the ESR cavity. After about 16 degradation and annealing cycles the annealed spin density is about 1.5 times larger than the as-deposited spin density. The spin density of the degraded sample increases at a much slower rate.

cycle, respectively. ESR spin densities measured after low-temperature degradation are not shown. Since the detected ESR signal is very sensitive to the sample position inside the ESR cavity, we again ascribe the scattering in the data mostly to slightly varying sample positions inside the cavity. However, a slight increase of the spin densities in the sample for both the annealed state and the degraded state can be identified. The densities of stable defects increase with the number of degradation and annealing cycles. The ESR line shape of the stable defects is identical with that of the metastable defects indicating that both are due to the same generic defect. In addition, the spin density of the degraded sample increases at a slower rate per cycle than the spin density of the annealed sample. Therefore, the difference in the spin densities between the degraded and annealed states decreases with increasing cycles. This result also means that annealing for 30 min at 175 °C does not fully restore the as-deposited spin density and that the optically induced defect creation becomes less efficient after many degradation and annealing cycles.

Although this effect also affects the previous data of Figs. 3 and 4, within the number of cycles performed in this work, the errors due to any increase in the stable defects that cannot be annealed at 175 °C or to any decrease in the efficiency of degradation are much smaller than the uncertainty in the data due to varying sample positions inside the cavity. We have therefore neglected these errors in presenting the data in Figs. 3 and 4.

DISCUSSION

Infrared quenching of long-lived carriers has frequently been used to quench, or bleach, the long-lived carriers in *a*-Si:H.[6,23,28,29] Our results clearly show that whereas quenching with typical photon energies of 0.5 eV strongly reduces the long-lived carriers, a small, but significant, fraction of long-lived carriers remains. Presumably, it is the most deeply trapped carriers in the conduction- and valence-band tails that are most difficult to remove optically. As the densities of trapped carriers get smaller, the probability that optical reexcitation will result in recombination is reduced relative to the probability for retrapping. These remaining, long-lived carriers can still be detected with ESR, but PL and PC measurements cannot detect them. The PL intensity is proportional to the rate of recombination of optically excited carriers, which rapidly decreases within a few minutes after the beginning of ir quenching. After a new, lower density of long-lived carriers is reached the PL becomes undetectably small. PC depends on mobile carriers. Since the optically excited carriers that survive ir quenching are deeply trapped, these carriers are also not detectable in PC. Only ESR, which directly measures the concentration of the long-lived carriers, is sensitive enough to detect these residual carriers.

We have carefully considered the remaining long-lived carriers, since they are difficult to distinguish from the optically excited silicon dangling bonds that contribute to the SWE and they exhibit similar growth kinetics: i.e., they follow a power law in time t as $t^{1/3}$. A similar dependence on time of the increase in subband-gap absorption, $\Delta\alpha/\alpha$, as measured by photoconductivity ($\Delta\alpha/\alpha \propto t^{1/3}$) has been observed at low temperatures, but in this case the increase was attributed to the production of defects contributing to the SWE.[6,29] We find that the production of silicon dangling bonds below 100 K is reduced by at least a factor of 2 from the degradation produced at room temperature. In fact, within experimental error this reduction could be more than a factor of 10.

Our degradation measurements are in qualitative, if not quantitative, agreement with those obtained by Stradins and Fritzsche[11] using a technique based on photoconductivity [so-called constant photocurrent method (CPM)]. Previous results from photoconductivity experiments[6,11] suggested that the production of defects at 4.2 K is about 70% of the value at 300 K. By directly measuring the optically induced ESR spin increase on a powdered sample, Yoshida and Taylor[30] found that the optically induced silicon dangling bond production at 40 K was approximately half as efficient as at 300 K. These results are in quantitative agreement with the present data. Finally, the low-energy PL band at 0.8 eV, which is commonly ascribed to radiative recombination through the dangling bonds, is much more enhanced after optical excitation at 300 K than at 40 K.[30] This result is also in qualitative agreement with the present data.

The defects that are created at low temperatures, e.g., at 25 K, almost completely anneal at room temperature, whereas the defects created at room temperature only anneal at about 420 K. This result implies that the annealing efficiency at a given temperature depends not only on the annealing temperature, but also on the defect creation temperature. This result also indicates that defects with differing stabilities are created at low and high temperatures. However, since ESR is one of the most sensitive tools for measuring the microscopic nature of defects and all the defects exhibit the same ESR line shape, one must conclude that the differences between the defects created at low and high temperatures do not involve significant differences in the wave functions for the trapped electrons. It is probable that the same defects—namely, the silicon dangling bonds—are created at both high and low temperatures, but that the stabilizing process is temperature dependent. This interpretation means that defects created at low temperatures, e.g., below 100 K, are less stabile and, therefore, anneal at lower temperatures than defects created at higher temperatures.

The results of the degradation and annealing cycling experiments suggest that there are a few defects that eventually survive annealing even at 175 °C. These defects are also undistinguishable from the other defects by ESR, again showing that only one defect is created at all temperatures, but that different stabilization mechanisms exist.

The defects are more stable when they are created at higher temperatures. Therefore, the stabilization process and the annealing process are correlated and both depend on the temperature. One might speculate that both the stabilization and annealing processes are thermally activated. If this assumption is correct, then almost all defect stabilization processes are totally inaccessible in at sufficiently low temperatures and degradation should not occur. However, our results are not accurate enough to prove this prediction. Our results

are also not accurate enough to prove that different, i.e., nonthermally activated, stabilization processes contribute to the SWE at low temperatures.

Over the years several models have been proposed to explain the SWE. One prominent model[27] assumes that nonradiative recombination can occur either between localized band tail states in the conduction and valence bands or through silicon dangling bond defects that are located deep within the optical or electronic energy gap. Because the localized states in the conduction- and valence-band tails are attributed to strained Si-Si bonds,[27] the first process provides an inefficient mechanism for the production of additional silicon dangling bonds by breaking strained Si-Si bonds. Presumably, a process involving the motion of hydrogen atoms separates these two dangling bonds from each other. A second recent model[12,13] involves the optically induced promotion of hydrogen, which is bonded to silicon, into states, such as bond-centered or interstitial sites, where the hydrogen can diffuse easily. This diffusion also provides an inefficient mechanism for the production of silicon dangling bonds in those unlikely cases where two diffusing hydrogen atoms come close enough together to produce a more deeply trapped, metastable defect involving both hydrogens, such as an analog of the H_2* defect in crystalline silicon.[31] As currently envisioned, neither of these models is robust enough to explain the decreased probability for the production of silicon dangling bonds at low temperatures coupled with the almost complete annealing of the low-temperature defects at 300 K. On the one hand, if the diffusion of hydrogen is temperature independent, then the kinetics of the effect should not change appreciably at low temperatures in contrast to the present results. On the other hand, if the diffusion of hydrogen is temperature dependent, it is hard to explain why the kinetics are essentially temperature independent below about 100 K. Clearly, the present results require more detailed model interpretations.

SUMMARY

In summary, low-temperature experiments that measure the production of silicon dangling bonds must take great care to remove the long-lived carriers trapped in localized band-tail states. These carriers are very difficult to remove optically and accumulate with the same kinetics as commonly observed for the SWE. The production of silicon dangling bonds in *a*-Si:H is at most half as efficient at 25 K as at 300 K and is only weakly temperature dependent below 100 K. In addition, essentially all of the defects created after 10 h of irradiation below 100 K anneal at 300 K. As commonly observed, defects created at about 300 K anneal at about 420 K. After many degrading and annealing cycles, a small fraction of defects survives annealing even at 175 °C for 30 min. This result shows that the SWE is not fully reversible with the standard annealing procedure. All optically induced defects, i.e., (i) those created at low temperatures, which anneal at about 300 K, (ii) those created at room temperature, which anneal at about 420 K, and (iii) those that survive annealing at 420 K, exhibit the same ESR line shape, indicating that only one type of defect is created. Also, these optically induced defects are indistinguishable from the inherent defects of the as-deposited sample. Therefore, the stabilization process alone, which must be temperature dependent, determines the nature of the defect. Any theoretical models of the SWE must account for these facts.

ACKNOWLEDGMENTS

The authors thank Z. V. Vardeny for helpful discussions and W. Wingert for help in sample preparation. We also thank P. Stradins and H. Fritzsche for insightful comments on the manuscript. This study was supported by NREL under subcontract Nos. XAK-8-17619-13 and ADJ-2-30630-23 and by the NSF under Grant No. DMR-0073004.

[1] D. L. Staebler and C. R. Wronski, Appl. Phys. Lett. **31**, 292 (1977).
[2] H. Dersch, J. Stuke, and J. Beichler, Appl. Phys. Lett. **38**, 456 (1980).
[3] M. H. Brodsky and R. S. Title, Phys. Rev. Lett. **23**, 581 (1969).
[4] X. Zou, Y. C. Chan, D. B. Webb, Y. W. Lam, Y. F. Hu, C. D. Beling, S. Fung, and H. M. Weng, Phys. Rev. Lett. **84**, 769 (2000).
[5] D. K. Biegelsen and M. Stutzmann, Phys. Rev. B **33**, 3006 (1986).
[6] P. Stradins and H. Fritzsche, Philos. Mag. B **69**, 121 (1994).
[7] W. B. Jackson, J. M. Marshall, and M. D. Moyer, Phys. Rev. B **39**, 1164 (1989).
[8] G. T. Barkema and N. Mousseau, Phys. Rev. Lett. **81**, 1865 (1998).
[9] R. Biswas and Y.-P. Li, Phys. Rev. Lett. **82**, 2512 (1999).
[10] N. Schultz and P. C. Taylor, in *Amorphous and Heterogeneous Silicon Thin Films: Fundamentals to Devices—1999*, edited by H. M. Branz, *et al.*, Mater. Res. Soc. Symp. Proc. No. **557** (Materials Research Society, Pittsburgh, 1999), p. 353.
[11] P. Stradins and H. Fritzsche, J. Non-Cryst. Solids **198–200**, 432 (1996).
[12] H. Branz, Solid State Commun. **105**, 387 (1998).
[13] S. B. Zhang and H. M. Branz, Phys. Rev. Lett. **84**, 967 (2000).
[14] R. A. Street and D. K. Biegelsen, Solid State Commun. **44**, 501 (1982).
[15] R. Carius and W. Fuhs, in *Optical Effects in Amorphous Semiconductors*, edited by P. C. Taylor and S. G. Bishop, AIP Conf. Proc. No. 120 (AIP, New York, 1984), p. 125.
[16] P. Persans, Philos. Mag. B **46**, 435 (1982).
[17] M. Q. Tran, P. Stradins, and H. Fritzsche, in *Amorphous Silicon Technology—1994*, edited by E. A. Schiff *et al.*, Mater. Res. Soc. Symp. Proc. No. 334 (Materials Research Society, Pittsburgh, 1994), p. 431.
[18] H. Fritzsche, S. Heck, and P. Stradins, J. Non-Cryst. Solids **198–200**, 153 (1996).
[19] F. Boulitrop, in *Optical Effects in Amorphous Semiconductors* (Ref. 15), p. 178.
[20] B. Yan and P. C. Taylor, in *Amorphous and Microcrystalline Silicon Technology—1998*, edited by S. Wagner *et al.*, Mater. Res.

Soc. Symp. Proc. No. 507 (Materials Research Society, Pittsburgh, 1997), p. 789.

[21] B. Yan, N. Schultz, A. L. Efros, and P. C. Taylor, Phys. Rev. Lett. **84**, 4180 (2000).

[22] M. Hoheisel, R. Carius, and W. Fuhs, J. Non-Cryst. Solids **59&60**, 457 (1983).

[23] P. Persons, Philos. Mag. B **46**, 435 (1982).

[24] X. Yin, J. M. Viner, S. Q. Gu, M. E. Raikh, and P. C. Taylor, Phys. Rev. B **49**, 5073 (1994).

[25] X. Yin, M. E. Raikh, and P. C. Taylor, in *Amorphous Silicon Technology—1995*, edited by M. Hack, E. A. Schiff, A. Madan, M. Powell, and A. Matsuda, Mater. Res. Soc. Symp. Proc. No. 377 (Materials Research Society, Pittsburgh, 1995), p. 167.

[26] See, for example, D. L. Griscom, Phys. Rev. B **20**, 1823 (1979).

[27] M. Stutzmann, W. B. Jackson, and C. C. Tsai, Phys. Rev. B **32**, 23 (1984).

[28] P. E. Vanier, A. E. Delahoy, and R. W. Griffith, J. Appl. Phys. **52**, 5235 (1981).

[29] P. Stradins and H. Fritzsche, in *Amorphous and Microcrystalline Silicon Technology—1997*, edited by S. Wagner *et al.*, Mater. Res. Soc. Symp. Proc. No. 1997 (Materials Research Society, Pittsburgh, 1997), p. 85.

[30] M. Yoshida and P. C. Taylor, in *Amorphous Silicon Technology—1992*, edited by M. J. Thompion *et al.*, Mater. Res. Soc. Symp. Proc. No. 258 (Materials Research Society, Pittsburgh, 1992) p. 347.

[31] See, for example, C. G. Van de Walle, in *Hydrogen in Semiconductors and Metals*, edited by N. H. Nichel *et al.*, Mater. Res. Soc. Symp. Proc. No. 513 (Materials Research Society, Warrendale, PA, 1998), p. 55.